Nuclear Science and Techniques (2023) 34:8
https://doi.org/10.1007/s41365-022-01160-5

Performance of real-time neutron/gamma discrimination methods

Shi-Xing Liu[1] · Wei Zhang[2] · Zi-Han Zhang[1] · Shuang Lin[2] · Hong-Rui Cao[3] · Cheng-Xin Song[2] · Jin-Long Zhao[3] · Guo-Qiang Zhong[3]

Received: 9 July 2022 / Revised: 23 November 2022 / Accepted: 24 November 2022 / Published online: 16 January 2023

Abstract
Nuclear security usually requires the simultaneous detection of neutrons and gamma rays. With the development of crystalline materials in recent years, $Cs_2LiLaBr_6$ (CLLB) dual-readout detectors have attracted extensive attention from researchers, where real-time neutron/gamma pulse discrimination is the critical factor among detector performance parameters. This study investigated the discrimination performance of the charge comparison, amplitude comparison, time comparison, and pulse gradient methods and the effects of a Sallen–Key filter on their performance. Experimental results show that the figure of merit (FOM) of all four methods is improved by proper filtering. Among them, the charge comparison method exhibits excellent noise resistance; moreover, it is the most suitable method of real-time discrimination for CLLB detectors. However, its discrimination performance depends on the parameters t_s, t_m, and t_e. When t_s corresponds to the moment at which the pulse is at 10% of its peak value, t_e requires a delay of only 640–740 ns compared to t_s, at which time the potentially optimal FOM of the charge comparison method at 3.1–3.3 MeV is greater than 1.46. The FOM obtained using the t_m value calculated by a proposed maximized discrimination difference model (MDDM) and the potentially optimal FOM differ by less than 3.9%, indicating that the model can provide good guidance for parameter selection in the charge comparison method.

Keywords Charge comparison · Maximized discrimination difference model · Pulse filtering · Real time · n-γ discrimination

1 1 Introduction

Neutron and gamma detection is an essential technique for many nuclear security applications, such as isotope identification [1, 2], radiation monitoring [3–5], and the search for fissile material [6, 7]. The detection of neutrons and gamma rays usually requires a combination of both types of radiation detectors, which must be portable and compact in many detection scenarios. In recent years, a new $Cs_2LiLaBr_6$(CLLB) detector in the elpasolite scintillator family has been developed [8]. It has the advantages of small size, high light output, and excellent energy resolution; it enables the detection of two types of radiation using pulse shape discrimination technology, making handheld instruments possible [9–12]. Since the 1960s, researchers have found that scintillators produce different pulse shapes when they interact with different particles [13], and many methods of discriminating the waveform characteristics have been developed. These methods are divided into three categories: time-domain, frequency-domain, and intelligent methods. Time-domain methods include charge comparison [14] (CC), time comparison (TC), amplitude comparison (AC), and pulse gradient (PG) methods [15]. Frequency-domain methods include frequency gradient [16], wavelet transform [17], and fractal spectrum [18] methods. Intelligent methods include multilayer perceptron [19], support vector machine [20,

This work was supported by cooperation projects between an enterprise (CNPE) and a research institute (ASIPP) (Y15HX16706).

✉ Shi-Xing Liu
liusx@hfut.edu.cn

✉ Wei Zhang
zhangweid@cnpe.cc

✉ Hong-Rui Cao
caohr@ipp.ac.cn

[1] School of Electronics, Hefei University of Technology, Hefei 230009, China

[2] China Nuclear Power Engineering Co., Ltd, Beijing 100840, China

[3] Institute of Plasma Physics, Hefei Institutes of Physical Science, Chinese Academy of Sciences, Hefei 230031, China

21], and deep learning network [22] approaches. Time-domain methods are simple to calculate but usually have a low figure of merit (FOM). Frequency-domain methods involve many Fourier calculations that are complex and difficult to run in real time; however, they are less sensitive to noise than time-domain methods. Intelligent methods usually have the highest FOM but require many floating-point matrix operations and thus a complicated computational process. In addition, the discrimination performance of intelligent methods usually depends on the training set size and number of neural network parameters. It is almost impossible to complete the computations required by frequency-domain and intelligent methods using limited computational and storage resources. In addition, as the sample points of the waveform increase, the computational complexity of frequency-domain and intelligent methods can rarely maintain linear growth. Therefore, time-domain methods are still preferred for real-time analysis. Consequently, it is necessary to study suitable discrimination methods and preprocessing techniques to identify methods with a good FOM and some noise immunity that are suitable for real-time analysis using modest computational resources. Zuo et al. [23] explored the discrimination effect of several time-domain methods on plastic scintillator detectors and found that filtering could enhance the discrimination performance of these methods. However, the applicability of this finding to CLLB detectors is unknown. In addition, time-domain methods are all sensitive to their parameters. To optimize the discrimination performance of these methods, one must continuously search for the appropriate parameters by trial and error, which is very laborious.

To solve these problems, we examine the discrimination effects of the CC, TC, AC, and PG time-domain methods on CLLB detectors and the effects of preprocessing by a Sallen–Key (SK) filter on the methods in real time. A new SK recursive expression based on the second-order Runge–Kutta method is proposed to reduce the error and applied in an experiment. The experimental results show that appropriate filtering can enhance the discrimination performance of these time-domain methods, where the CC method is the most suitable real-time analysis method for CLLB detectors. However, the performance of the CC method is affected by the parameter settings. We discuss the effects of the CC parameters on its discrimination performance and propose a maximized discrimination difference model (MDDM) to guide parameter selection in the CC method. This tool can be used to model the parameter settings of other time-domain methods and guide parameter selection.

The remainder of the paper is organized as follows. The experimental setup for the work is described in Sect. 2. The basic principles of the numerical methods used are described in Sect. 3. The discrimination effects of the methods and the effects of filtering and the MDDM on their performance are discussed in Sect. 4. Conclusions are presented in Sect. 5.

2 Neutron/gamma pulse discrimination experiment

2.1 Detector and radioactive source

A CLLB crystal detector from Saint-Gobain [24] was used; the scintillator crystal has a diameter of 2 in. and is sealed inside an aluminum housing. It was coupled directly to a photomultiplier tube (PMT) (Hamamatsu R6231-100), as shown in Fig. 1. An ORTEC 556 high-voltage power supply was used during the experiment to supply a voltage of 800 V to the detector. A ^{137}Cs gamma source was used as the energy calibration source for the detector, and a ^{252}Cf source was selected to provide the neutron/gamma hybrid radiation field.

2.2 Data acquisition system

A data acquisition system developed by our research group was used for the experiment; it includes a PXIe chassis with an embedded controller and an electronics card. The signal input of the main electronics card was directly connected to the CLLB detector. The main electronics card consists mainly of analog signal conditioning components, high-speed analog-to-digital converters (ADCs) (14 bits and 500 Msps), a clock jitter cleaner, and a field-programmable gate array (FPGA) (type xc7k325tffg900). As shown in Fig. 4, the rise time of the electrical signal of the CLLB detector is $t_r \geq 30$ ns. If the signal is processed directly by a 500 Msps ADC, there are no fewer than 15 sampling points on the rising edge. A signal with a rising edge $t_r = 30$ ns corresponds to the frequency spectrum of 16.7 MHz, which is much lower than the sampling rate of the waveform digitization module for 500 Msps ADCs. The hardware of the main electronics card is almost identical to

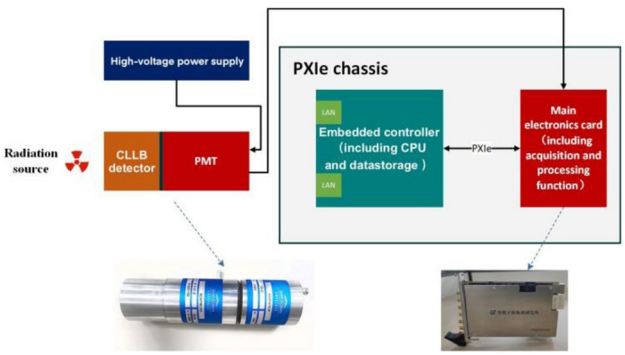

Fig. 1 Neutron/gamma signal discrimination system based on CLLB detector

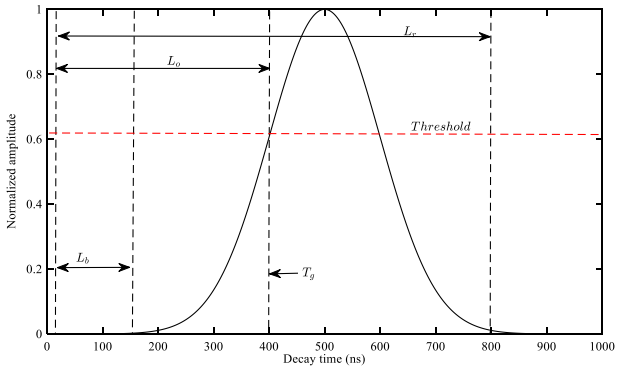

Fig. 2 Pulse recording mode

that of the main electronics card for neutron flux monitoring in the Experimental Advanced Superconducting Tokamak [25], except that the gain of the analog signal conditioning component is 8 V/V to accommodate the signal amplitude of the CLLB detector and PMT output (< 100 mV), and the FPGA code is different. Data processed by the FPGA algorithm are transmitted to the chassis-embedded controller through the PXIe bus in direct memory access mode for display or storage [26].

The pulse acquisition mode of the FPGA is shown in Fig. 2. L_r is the length of the entire recorded pulse; L_b is the length of the sliding average of the baseline calculation; L_o is the offset of the pulse trigger, which determines the starting point of the baseline calculation; and T_g is the moment at which the pulse is triggered. In this experiment, the average value of 48–64 ns sampling points before pulse triggering was defined as the baseline of the pulse, and the total recording time of the pulse was 1008 ns.

2.3 Pulse preprocessing

First, the detector was energy-calibrated using a ^{137}Cs gamma source. Then, a pulse waveform with an equivalent gamma energy of 3.1–3.3 MeV (the energy band containing the thermal neutron peak) was extracted from the ^{252}Cf source; therefore, we investigated the neutron/gamma discrimination performance in this energy band. A total of 33,782 waveforms were measured. Pulse width and amplitude analysis was used to remove severely overlapped or chopped waveforms; 33, 246 pulse waveforms remained after this process. Finally, each pulse baseline value was subtracted from the sampled pulse sample data.

3 Principle of numerical method

3.1 SK filter

In 1955, the SK filter based on discrete components was first proposed by R.P. Sallen and E.L. Key, and the Gaussian shaping of pulse signals was successfully realized. SK filters are widely used for signal filtering and pulse shaping, where they outperform other methods in terms of energy resolution and computational workload [27]. The SK filter has a second-order filter circuit with a simple structure and is widely used in nuclear signal pulse shaping [28, 29]. Figure 3 shows the SK low-pass filter. When $R1 = R2 = R = 3.99$ kΩ and $C1 = C2 = C = 1.5$ pF, the corresponding bandwidth is 16.7 MHz.

3.2 Real-time discrimination method

The CC method uses the different integration values of the neutron and gamma pulse tails as the basis for discrimination. The principle is illustrated in Fig. 4a; the discrimination is calculated using Eq. (1):

$$P_{\mathrm{CI}} = \frac{Q - Q_{\mathrm{f}}}{Q} = \frac{Q_{\mathrm{s}}}{Q_{\mathrm{f}} + Q_{\mathrm{s}}}, \tag{1}$$

where Q is the total pulse integral, and Q_{f} and Q_{s} represent the pulse front and tail integrals, respectively. The range of the integration intervals of Q_{f} is determined by t_{s} and t_{m}, and the integration interval of Q is determined by t_{s} and t_{e}. If the interval between t_{s} and t_{m} is set too large, it will cause a loss of the difference between the falling portions of the neutron and gamma pulse signals in Eq. (1), where P_{CI} thus tends to 0. By contrast, if the interval between t_{s} and t_{m} is set too small, the information on useless pulses in Eq. (1) will increase, causing P_{CI} to tend to 1. Therefore, the integration

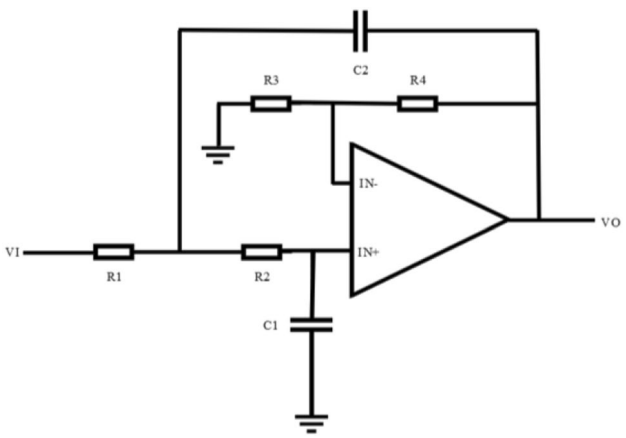

Fig. 3 Schematic diagram of SK low-pass filter

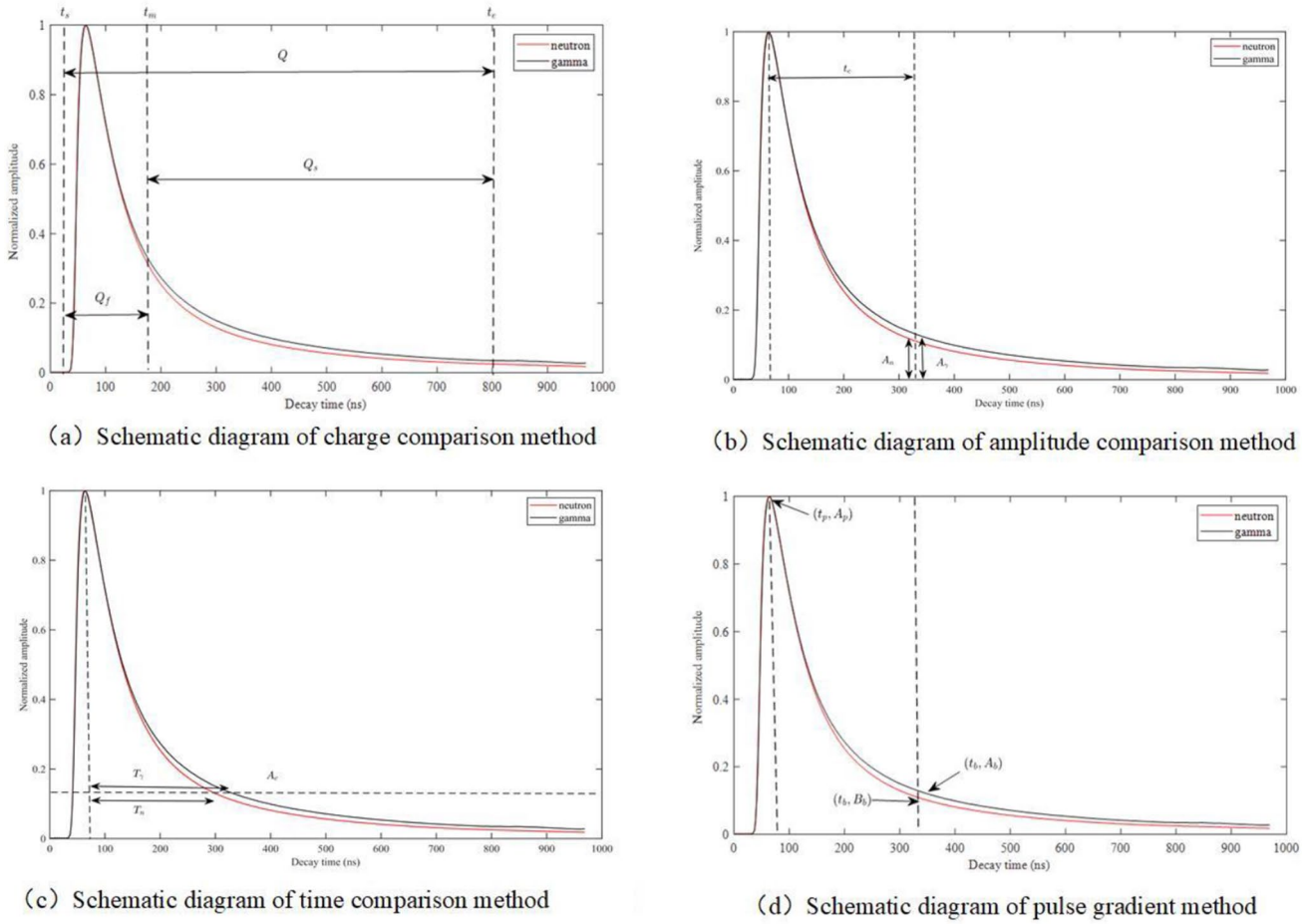

(a) Schematic diagram of charge comparison method

(b) Schematic diagram of amplitude comparison method

(c) Schematic diagram of time comparison method

(d) Schematic diagram of pulse gradient method

Fig. 4 (Color online) Schematic diagram of discrimination methods

interval needs to be selected according to the pulse waveform of the detector response in practical applications. In the CLLB detector, the neutron pulse will have smaller P_{CI} values than the gamma pulse because neutrons decay faster than gammas, unlike the typical case of liquid scintillators.

The principle of the AC method is shown in Fig. 4b, where t_c after the peak is selected as the moment of amplitude comparison. The different amplitudes of neutrons and gammas at this moment are used as the basis for discrimination, where A_γ and A_n represent the amplitude of the gamma and neutron pulses, respectively, at the t_c moment. This method requires the calculation of only one sampling point but is very susceptible to the effects of noise. Therefore, the amplitudes were normalized before comparison with the other methods.

The principle of the TC method is shown in Fig. 4c. It can be considered as the inverse function of the AC method. A fixed A_c threshold line is chosen, and the difference in the time it takes for neutron and gamma pulses to decay from their peaks to the threshold line is used as the basis for discrimination. T_γ and T_n represent the time from the intersection of the decaying portion of the gamma and neutron pulse, respectively, with the threshold line A_c to the peak.

The PG method selects peak and post-peak sampling points for gradient calculation; the principle is illustrated in Fig. 4d. It can be written as Eq. (2):

$$P_G = \frac{A_p - A_b}{t_p - t_b}, \tag{2}$$

where P_G is the pulse gradient, A_p is the pulse peak amplitude, and A_b is the amplitude at a specific time interval after the pulse peak. In addition, t_p and t_b are the corresponding moments of the pulse peak and post-peak sampling points, respectively. Similarly, the gradient is susceptible to strong amplitude effects and is calculated using normalized amplitudes.

3.3 Evaluation criteria

The FOM was introduced as an evaluation criterion to objectively assess the performance of the discrimination method, as shown in Fig. 5. The FOM is defined [30] as shown in Eq. (3):

$$\mathrm{FOM} = \frac{D}{\mathrm{FWHM_n} + \mathrm{FWHM}_\gamma}, \tag{3}$$

$\mathrm{FWHM_n}$ and FWHM_γ are the half-height widths of the neutron and gamma peaks, respectively, and D is the distance between the neutron and gamma peaks. A larger FOM indicates that the method exhibits better neutron/gamma discrimination.

3.4 MDDM

Among the four methods described above, only the CC method uses all the waveform information. Therefore, it has better noise immunity. The discrimination performance of the CC method depends on three parameters, t_s, t_m, and t_e. The values of t_s and t_e are usually taken as the moments of the upper edge of the pulse and the end of pulse decay, respectively, and the parameter t_m is the most difficult to determine. We propose a model that maximizes the difference used for discrimination to determine the parameter t_m and achieve excellent performance by the CC method. When neutrons and gamma rays deposit energy in the CLLB detector, the photon pulse generated by the scintillation crystal can be written as shown in Eq. (4).

$$I(t) = I_f e^{-t/\tau_f} + I_s e^{-t/\tau_s}, \tag{4}$$

where τ_f and τ_s are the fast and slow components of the decay time constant, respectively. I_f and I_s represent the proportions of the fast and slow components, respectively.

In the linear region, the pulse output from the CLLB detector can be represented by the convolution of the photon pulse with the response function of the PMT and readout electronics. However, the final expression of $V(t)$ still contains the factors e^{-t/τ_f} and e^{-t/τ_s} [31]. Because the pulse rises rapidly, this part of the output can be replaced by a linear function; thus, the gamma and neutron pulse response described above can be written as shown in Eqs. (5) and (6), respectively.

$$V_{\mathrm{CLLB}\gamma}(t) = \begin{cases} K_\gamma t, \ t < t_1 \\ A(I_{f\gamma} e^{-(t-t_1)/\tau_f} + I_{s\gamma} e^{-(t-t_1)/\tau_s}), \ t \geq t_1 \end{cases} \tag{5}$$

$$V_{\mathrm{CLLBn}}(t) = \begin{cases} K_n t, \ t < t_1 \\ A(I_{fn} e^{-(t-t_1)/\tau_f} + I_{sn} e^{-(t-t_1)/\tau_s}), \ t \geq t_1 \end{cases} \tag{6}$$

$$K_\gamma = K_n = A/t_1 \tag{7}$$

$I_{f\gamma}$ and $I_{s\gamma}$ represent the fast and slow components, respectively, of the pulse response to gamma rays. I_{fn} and I_{sn} represent the fast and slow components, respectively, of the response to neutrons. A is the response amplitude, which is proportional to the ray energy. In the actual detector impulse response, the pulse first rises and then decays, as shown in Fig. 6.

The rise time of the CLLB response pulse to the peak is the same for rays of different energies. t_0, t_1, and t_2 represent the moments at which the pulse starts to rise, reaches its peak, and is completely decayed, respectively. S_a represents the pulse integration area of the neutron and gamma pulses from t_0 to t_1. Neutrons and gammas of the same energy in the rising phase of the pulse can be considered to have the same integration area. S_b represents the integration area of the neutron pulse from t_1 to t_2. Because the slow component of the gamma response pulse is more significant in the decaying part of the pulse, S_c represents the excess integration area of the gamma pulse from t_1 to t_2 compared to the neutron pulse. The P_{CI} values of gammas and neutrons in the CC method are calculated as shown in Eqs. (8) and (9), respectively:

$$P_{\mathrm{CI}\gamma} = \frac{S_b + S_c - S_{\gamma\delta}}{S_a + S_b + S_c}, \tag{8}$$

$$P_{\mathrm{CIn}} = \frac{S_b - S_{n\delta}}{S_a + S_b}. \tag{9}$$

The difference in P_{CI} between neutrons and gammas is strongly correlated with D in Eq. (3). Therefore, the FOM of the CC method is expected to be highest when $\delta = t_1 + \tau_m$ reaches the moment at which the difference in P_{CI} between neutrons and gammas is maximum.

$$D(\delta) = P_{\mathrm{CI}\gamma} - P_{\mathrm{CIn}} = \frac{S_{n\delta}(S_a + S_b + S_c) - S_{\gamma\delta}(S_a + S_b) + S_a S_c}{(S_a + S_b + S_c)(S_a + S_b)} \tag{10}$$

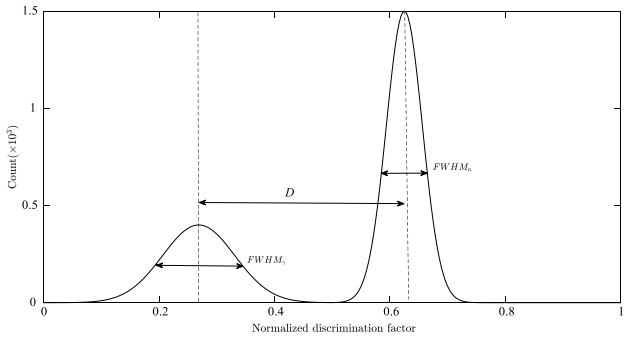

Fig. 5 Criteria for evaluating neutron/gamma discrimination

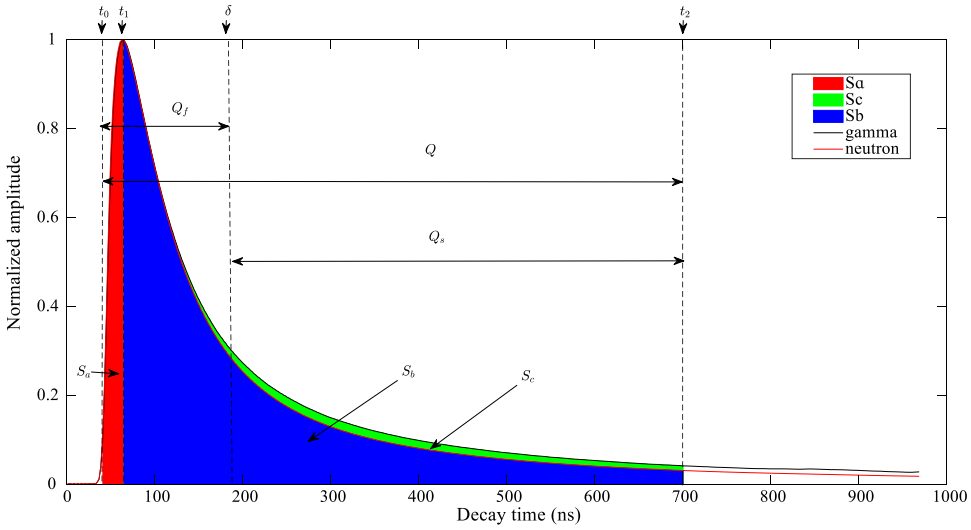

Fig. 6 (Color online) Model of output pulse response of CLLB detector

If $I_{f\gamma} < I_{fn}, I_{s\gamma} > I_{sn}$ and $0 < \tau_m < t_2 - t_1$, τ_m is the moment at which the difference between the P_{CI} values of gammas and neutrons is largest, as shown in Eq. (11).

$$\tau_m = \frac{\tau_f \tau_s}{\tau_s - \tau_f} \ln\left(\frac{I_{fn}p - I_{f\gamma}q}{I_{s\gamma}q - I_{sn}p}\right) \tag{11}$$

$$p = S_a + S_b + S_c, q = S_a + S_b, p < q \tag{12}$$

By calculating τ_m, the parameters of the CC method that will yield the best FOM can be obtained.

4 Experimental results and discussion

4.1 Comparison of methods

The discrimination effects of the time-domain methods discussed above are all related to the parameter values. To objectively evaluate each method, the definition domain of the discrimination parameters of each method is first given. Then the best FOM using these parameters is obtained as the discrimination performance of the method by a trial-and-error approach. Let t_s be 10% of the time required for the pulse to rise to its peak, t_p be the moment of the pulse peak, and t_e be 700 ns after t_s. For the CC method, t_m satisfies Eq. (13); for the AG method, t_c satisfies Eq. (14); for the PG method, t_b satisfies Eq. (15); and for the TC method, the A_c range is taken from 0.1 to 1 peak, at intervals of 1% of the peak.

$$t_s < t_m < t_e \tag{13}$$

$$t_p < t_c < t_e \tag{14}$$

$$t_p < t_b < t_e \tag{15}$$

The FOM of the methods without filtering is shown in Fig. 7. Only the CC method can distinguish between neutron and gamma pulses at the current noise level, where the parameter t_m is taken as 212 ns after t_s to obtain the best FOM for this method.

As show in Fig. 3, the shaping effect of the SK low-pass filter is affected by the value of *RC*. With increasing *RC*, the cutoff frequency decreases, the attenuation of the stop-band increases, and the filtering effect is improved.

The AC method is more strongly affected by noise, which is strongly correlated with the filtering effect. The overall FOM of the TC method is low; it is challenging to distinguish neutron and gamma signals correctly because the shaped pulse has a large oscillation with time. Therefore, the TC method is not suitable for neutron/gamma discrimination.

The PG method is also more strongly affected by noise. The FOM of the PG method is strongly correlated with the filtering effect. In addition, the FOM of the PG method is similar to that of the AC method because of the amplitude difference in Eq. (3) in the calculation, which indicates that the amplitude difference is the dominant factor in discrimination by the PG method.

Therefore, the CC method is the most suitable processing method for real-time neutron/gamma discrimination.

4.2 Effect of MDDM

When the t_s and t_e parameters of the CC method are fixed as described in Sect. 4.1, we take $t_m = \{t | t = 60 + 20 \times a, a = 0, 1, 2, 3, ..., 28\}$. The FOM of the CC method for these values of *tm* is shown in Fig. 8. The FOM curve is convex, which indicates the best FOM can be obtained by considering the FOM as a function of the single parameter t_m, and confirms the suitability of the

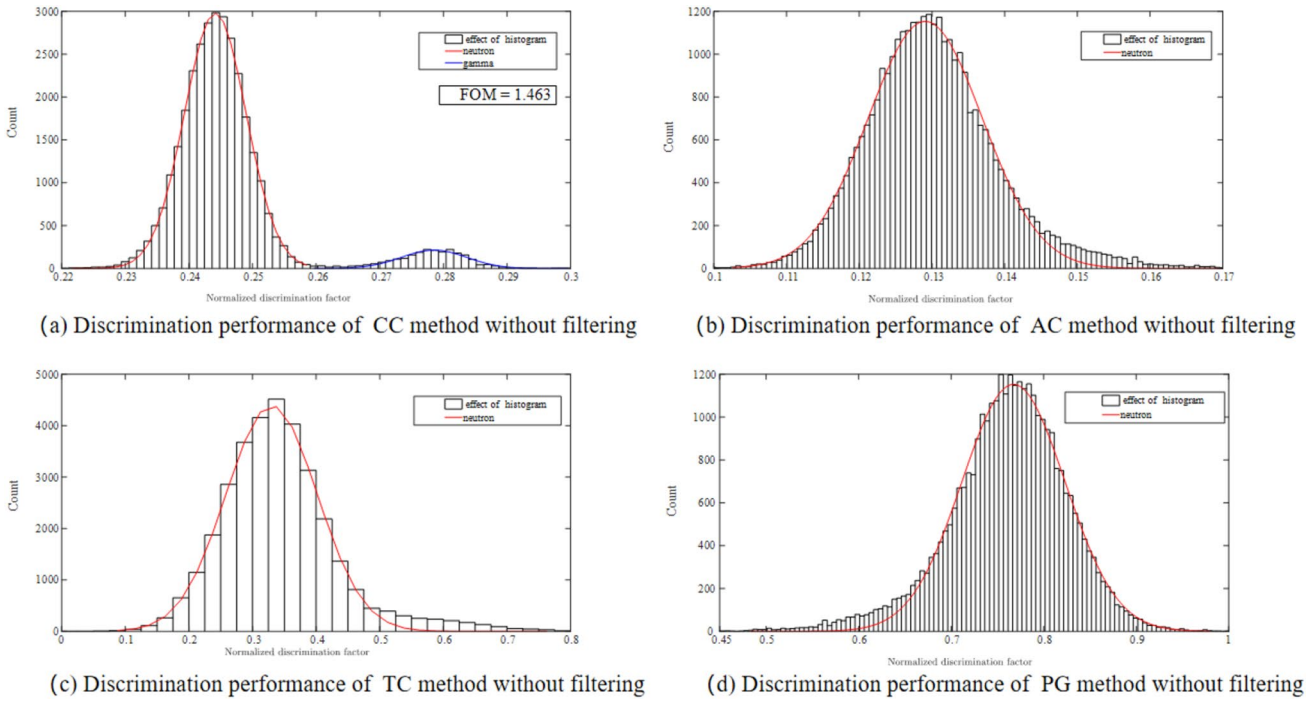

Fig. 7 Discrimination performance of different methods without filtering

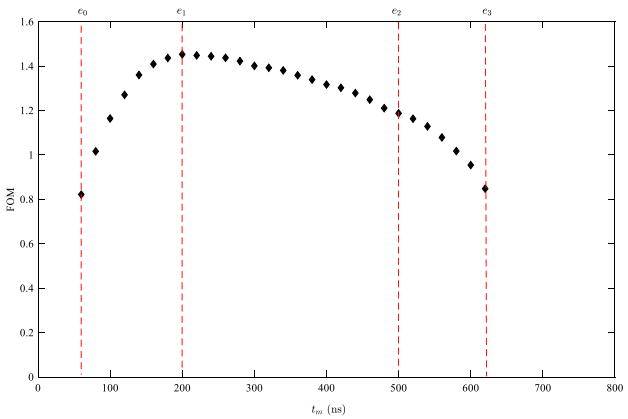

Fig. 8 Effect of t_m on FOM of CC method

MDDM proposed in Sect. 3.4. Let e_0-e_1 be the R_0 region, e_1-e_2 be the R_1 region, and e_2-e_3 be the R_2 region. The slope of the curves in the R_0 and R_1 regions is larger, indicating that the FOM improves more rapidly when t_m is close to e_1. By contrast, the FOM decreases rapidly when t_m is close to e_3. The slope of the curve in the R_2 region is smaller, indicating a slower decrease in the FOM in this region, although the range is large. Thus, the performance of the CC method is somewhat independent of the t_m value.

To solve Eq. (11) for τ_m, only I_{fn}, I_{sn}, $I_{f\gamma}$, $I_{s\gamma}$, τ_f, τ_s and t_1 need to be calculated. They were obtained by fitting the neutron/gamma pulse waveform by Eqs. (5) and (6), as follows:

1. The neutron/gamma pulse signals were extracted separately by the CC method (using the parameters that were used to achieve the performance shown in Fig. 7), where 2000 pulse waveforms each were extracted for neutrons and gammas.
2. The average waveforms of neutron and gamma pulses were calculated and fitted with Eqs. (5) and (6) for neutrons and gammas, respectively, to obtain τ_{fn}, τ_{sn}, $\tau_{f\gamma}$, and $\tau_{s\gamma}$.
3. The average of the rise times of the fitted neutron and gamma waveforms is obtained as $t_1 = 30$ ns.
4. The average of τ_{fn} and $\tau_{f\gamma}$ is taken as $\tau_f = 81.51$ ns, and the average of τ_{sn} and $\tau_{s\gamma}$ is taken as $\tau_s = 451.27$ ns.
5. By substituting τ_f and τ_s into Eqs. (5) and (6), we obtained $I_{fn} = 0.868, I_{sn} = 0.132, I_{f\gamma} = 0.837$, and $I_{s\gamma} = 0.163$.

We confirm that the above parameters satisfy Eq. (11). For a fixed value of t_s, we take $t_e = \{t | t = 300 + 20 \times a, a = 0, 1, 2, 3, \ldots, 30\}$. Figure 9 compares the FOM obtained using the t_m values calculated using the MDDM with the potentially optimal FOM for different *te* values. The potentially optimal FOM versus t_m curve (black dots) is still convex, indicating that t_e does not need to cover the entire pulse to obtain the best discrimination performance of the CC method, and thus the calculation time required for integration can be reduced. Experimental tests show that t_e can be set between 640 and 740 ns after t_s, where the potentially optimal FOM exceeds 1.46. In addition, when t_e is set in this

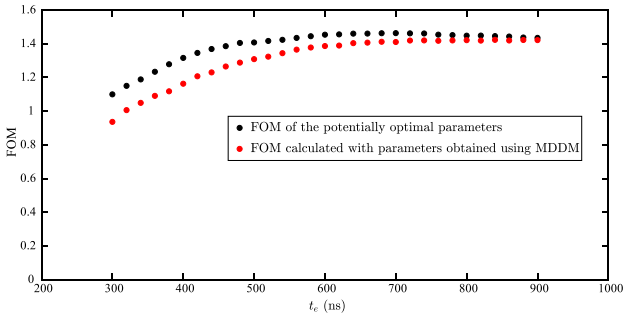

Fig. 9 Comparison of FOM obtained using MDDM and optimized parameters. The black dots represent the potentially optimal FOM for different values of t_e. The red dots represent the FOM obtained using the t_m values calculated using the MDDM for different values of t_e

range, the difference between the FOM obtained using the t_m value calculated using the MDDM and the potentially optimal FOM is less than 3.9%, confirming that it can improve the performance of the CC method.

5 Conclusion

This work studied the use of four real-time discrimination methods with CLLB detectors. The FOM of the four methods was improved when the pulses were adequately filtered. The CC method, with an excellent FOM and noise immunity, is the most suitable real-time discrimination method for CLLB detectors. Experimental tests showed that when t_s in the CC method is set to the moment at which the pulse rises to 10% of its peak, t_e should be within 640–740 ns after t_s to yield the potentially optimal FOM. In this parameter range, the FOM obtained using the t_m value calculated using the MDDM and the potentially optimal FOM differ by less than 3.9%. This result provides a good guide for parameter setting in the CC method. The concept of MDDM analysis can be used to model the parameters setting in other time-domain methods and provide guidance for parameter selection.

Acknowledgments The authors thank the ASIPP team for providing a suitable experimental environment for the radioactive source.

Author contributions All authors contributed to the study conception and design. Material preparation, data collection, and data analysis were performed by Shi-Xing Liu, Wei Zhang, Zi-Han Zhang, Shuang Lin, Hong-Rui Cao, Cheng-Xin Song, Jin-Long Zhao, and Guo-Qiang Zhong. The first draft of the manuscript was written by Zi-Han Zhang, and all authors commented on previous versions of the manuscript. All authors read and approved the final manuscript.

References

1. M. Kamuda, C.J. Sullivan, An automated isotope identification and quantification algorithm for isotope mixtures in low-resolution gamma-ray spectra. Radiat. Phys. Chem. **155**, 281–286 (2019). https://doi.org/10.1016/j.radphyschem.2018.06.017
2. Z. Varga, M. Wallenius, A. Nicholl et al., Assessment of uranium inhomogeneity and isotope imaging for nuclear forensics. Spectrochim Acta. B. **171**, 105920 (2020). https://doi.org/10.1016/j.sab.2020.105920
3. M.J. Zhou, L.Q. Hu, L.S. Huang et al., Measurement of the radiation dose distribution in EAST hall based on thermoluminescence dosimeter. Fusion. Eng. Des. **160**, 111977 (2020). https://doi.org/10.1016/j.fusengdes.2020.111977
4. Š Čerba, J. Lüley, B. Vrban et al., Unmanned radiation-monitoring system. IEEE T. Nucl. Sci. **67**(4), 636–643 (2020). https://doi.org/10.1109/TNS.2020.2970782
5. H.-R. Liu, Y.-X. Cheng, Z. Zuo et al., Discrimination of neutrons and gamma-rays in plastic scintillator based on pulse coupled neural network. Nucl. Sci. Tech. **32**(8), 82 (2021). https://doi.org/10.1007/s41365-021-00915-w
6. R.T. Kouzes, J.H. Ely, L.E. Erikson et al., Neutron detection alternatives to 3He for national security applications. Nucl. Instrum. Meth. A. **623**(3), 1035–1045 (2010). https://doi.org/10.1016/j.nima.2010.08.021
7. P.R. Menge, J. Lejay, V. Ouspenski.: Design and performance of a compact $Cs_2LiLaBr_6$(Ce) neutron/gamma detector using silicon photomultipliers. In: 2015 IEEE Nuclear Science Symposium and Medical Imaging Conference (San Diego, USA 31 Oct.-7 Nov. 2015)
8. J. Glodo, R. Hawrami, E.van Loef, et al., Pulse shape discrimination with selected elpasolite crystals. IEEE T. Nucl. Sci. **59**(5), 2328–2333 (2012). https://doi.org/10.1109/TNS.2012.2188646
9. J.E. van GlodoLoef, R. Hawrami, Selected properties of Cs_2LiYCl_6, $Cs_2LiLaCl_6$ and $Cs_2LiLaBr_6$ scintillators. IEEE T. Nucl. Sci. **58**(1), 333–338 (2011). https://doi.org/10.1109/TNS.2010.2098045
10. R.S. Woolf, B.F. Phlips, E.A. Wulf, Characterization of the internal background for thermal and fast neutron detection with CLLB. Nucl. Instrum. Meth. A. **838**, 147–153 (2016). https://doi.org/10.1016/j.nima.2016.09.013
11. R.S. Woolf, E.A. Wulf, B.F. Phlips et al., Identification of internal radioactive contaminants in elpasolites CLYC, CLLB, CLLBC and other inorganic scintillators. Nucl. Instrum. Meth. A. **954**, 161228 (2020). https://doi.org/10.1016/j.nima.2018.09.063
12. J.-L. Cai, D.-W. Li, P.-L. Wang et al., Fast pulse sampling module for real-time neutron-gamma discrimination. Nucl. Sci. Tech. **30**(5), 84 (2019). https://doi.org/10.1007/s41365-019-0595-1
13. F.D. Brooks, Development of organic scintillators. Nucl. Instrum. Methods. **162**(1–3), 477–505 (1979). https://doi.org/10.1016/0029-554X(79)90729-8
14. M. Moszynski, G. Bizard, G.J. Costa et al., Study of n-γ discrimination by digital charge comparison method for a large volume liquid scintillator. Nucl. Instrum. Meth. A. **317**(1–2), 262–272 (1992). https://doi.org/10.1016/0168-9002(92)90617-D
15. B.D. Mellow, M.D. Aspinall, R.O. Mackin et al., Digital discrimination of neutrons and γ-rays in liquid scintillators using

pulse gradient analysis. Nucl. Instrum. Meth. A. **578**(1), 191–197 (2007). https://doi.org/10.1016/j.nima.2007.04.174
16. G. Liu, M.J. Joyce, X. Ma et al., A digital method for the discrimination of neutrons and γ rays with organic scintillation detectors using frequency gradient analysis. IEEE T. Nucl. Sci. **57**(3), 1682–1691 (2010). https://doi.org/10.1109/TNS.2010.2044246
17. S. Yousefi, L. Lucchese, A wavelet-based pulse shape discrimination method for simultaneous beta and gamma spectroscopy. Nucl. Instrum. Meth. A. **599**(1), 66–73 (2009). https://doi.org/10.1016/j.nima.2008.10.026
18. M.Z. Liu, B.Q. Liu, Z. Zuo et al., Toward a fractal spectrum approach for neutron and gamma pulse shape discrimination. Chin. Phys. C **40**(6), 066201 (2016). https://doi.org/10.1088/1674-1137/40/6/066201
19. P.A. Söderström, G. Jaworski, J.J.V. Dobón et al., Neutron detection and γ-ray suppression using artificial neural networks with the liquid scintillators BC-501A and BC-537. Nucl. Instrum. Meth. A **916**, 238–245 (2019). https://doi.org/10.1016/j.nima.2018.11.122
20. M. Gelfusa, R. Rossi, M. Lungaroni et al., Advanced pulse shape discrimination via machine learning for applications in thermonuclear fusion. Nucl. Instrum. Meth. A **974**, 164198 (2020). https://doi.org/10.1016/j.nima.2020.164198
21. H. Arahmane, A. Mahmoudi, E.M. Hamzaoui et al., Neutron-gamma discrimination based on support vector machine combined to nonnegative matrix factorization and continuous wavelet transform. Measurement **149**, 106958 (2020). https://doi.org/10.1016/j.measurement.2019.106958
22. S. Woldegiorgis, A. Enqvist, J. Baciak, ResNet and CycleGAN for pulse shape discrimination of He-4 detector pulses: recovering pulses conventional algorithms fail to label unanimously. Appl. Radiat. Isotopes. **176**, 109819 (2021). https://doi.org/10.1016/j.apradiso.2021.109819
23. Z. Zuo, Y.L. Xiao, Z.F. Liu et al., Discrimination of neutrons and gamma-rays in plastic scintillator based on falling-edge percentage slope method. Nucl. Instrum. Meth. A **1010**, 165483 (2021). https://doi.org/10.1016/j.nima.2021.165483
24. CLLB.Handbook.https://www.crystals.saint-gobain.com/sites/hps-mac3-cma-crystals/files/2021-09/CLLB-Material-Data-Sheet.pdf
25. L. Yang, H.R. Cao, J.L. Zhao et al., Development of a wide-range and fast-response digitizing pulse signal acquisition and processing system for neutron flux monitoring on EAST. Nucl. Sci. Tech. **33**(35), 1–11 (2022). https://doi.org/10.1007/s41365-022-01016-y
26. Y.Y. Zheng, Z.H. Zhang, Q. Li et al., Design of an energetic particle radiation diagnostic spectroscopy system based on national core chips and Qt on Linux in EAST. Nucl. Sci. Tech. **32**, 68 (2021). https://doi.org/10.1007/s41365-021-00906-x
27. H.Q. Zhang, B. Tang, H.X. Wu et al., Study of Sallen-Key digital filters in nuclear pulse signal processing. Nucl. Sci. Tech. **30**(10), 145 (2019). https://doi.org/10.1007/s41365-019-0679-y
28. S. Saxena, A.I. Hawari, Investigation of FPGA-based real-time adaptive digital pulse shaping for high-count-rate applications. IEEE T. Nucl. Sci. **64**(7), 1733–1738 (2017). https://doi.org/10.1109/TNS.2017.2692219
29. W. Gao, S. Li, Y. Duan et al., Design and characterization of a low-noise front-end readout ASIC in 0.18- μm CMOS technology for CZT/Si-PIN detectors. IEEE T. Nucl. Sci. **65**(5), 1203–1211 (2018). https://doi.org/10.1109/TNS.2018.2826070
30. R.A. Winyard, J.E. Lutkin, G.W. McBeth, Pulse shape discrimination in inorganic and organic scintillators. I. Nucl. Instrum. Methods. **95**(1), 141–153 (1971). https://doi.org/10.1016/0029-554X(71)90054-1
31. Z.H. Wang, J. Zeng, T.H. Zhu et al., Optimization of integration limit in the charge comparison method based on signal shape function. Nucl. Instrum. Meth. A. **760**, 5–9 (2014). https://doi.org/10.1016/j.nima.2014.05.017